IRSTI 27.35.43 https://doi.org/10.26577/ijmph.20211926

STABILITY AND GLOBAL DYNAMICS OF A DISCRETE SEIR MODEL IN THE LOTKA-VOLTERRA FRAMEWORK

D. Eshmamatova [1,2*] **and D. Xakimova** [1]

[1] *Tashkent State Transport University, Tashkent, Uzbekistan*

[2] *V. I. Romanovskiy Mathematics Institute, Uzbekistan Academy of Sciences, Tashkent, Uzbekistan*

Email: 24dil@mail.ru

(Received 5 May 2026; revised 30 October 2026; accepted 6 November 2026)

Abstract. This work investigates a discrete SEIR-type epidemic model formulated as a Lotka-Volterra dynamical operator on the three-dimensional simplex. The model describes nonlinear interactions among susceptible, exposed, infectious, and recovered population fractions through latent and direct infection pathways. The qualitative dynamics are studied using spectral analysis of boundary fixed points, signature-based geometric decomposition, successive-iteration analysis, and a Lyapunov-type dissipation argument. The simplex is partitioned into four convex polyhedral signature regions, and their facet-adjacency structure is determined explicitly. One-step sign constraints and admissible transition directions are established, distinguishing geometric adjacency from actual dynamical transitions. The main global result proves that every trajectory starting in the interior of the simplex converges to a single point of a distinguished fixed boundary segment. Local spectral properties and infectious threshold conditions are investigated through the Jacobian matrix. Numerical experiments illustrate global convergence, dependence of limiting states on initial conditions and parameters, and transitions between signature regions. The results provide a geometric framework for understanding the qualitative dynamics of discrete interaction-based SEIR-type systems.

Keywords: SEIR model, Lotka-Volterra operator, signature method, global dynamics, stability

INTRODUCTION

Discrete epidemiological models of the SEIR type play an important role in the qualitative analysis of epidemic processes, since they allow one to describe the evolution of susceptible, exposed (latent), infectious, and recovered populations in a unified dynamical framework [1, 2, 3, 4].

In particular, Lotka-Volterra type operators acting on simplices have been shown to be an effective tool for studying nonlinear interaction mechanisms in population dynamics.

Several related studies have investigated fixed-point configurations of operators on simplices [5], discrete SIRD models based on Lotka-Volterra mappings [6], and degenerate discrete Lotka-Volterra systems with epidemiological applications [7]. These investigations provide a mathematical background for the study of invariant sets, fixed points, and asymptotic dynamics.

The present paper is devoted to the qualitative analysis of a discrete SEIR model [8, 9, 10] formulated as a Lotka-Volterra type operator acting on the three-dimensional simplex. Our main goal is to describe the global dynamics of the model by combining spectral analysis of fixed points with a geometric partition of the simplex based on signature techniques. This approach makes it possible to characterize the qualitative evolution of trajectories in terms of fixed sets, signature regions, and local transition directions.

The interaction structure of the model corresponds to the epidemiological transition graph $S \to E \to I \to R$ together with an additional direct infection pathway $S \to I$.

Thus, the interaction terms of the proposed operator describe both the latent pathway $S \to E \to I \to R$ and an additional direct pathway $S \to I \to R$.

Previous investigations of discrete epidemic models have addressed such questions as equilibrium stability, bifurcation, incidence mechanisms, and numerical evolution [4, 8, 10]. These approaches provide information about local epi-

 © 2026 Al-Farabi Kazakh National University

demiological dynamics, but they do not, by themselves, determine the geometry of the signature regions associated with the Lotka-Volterra operator considered here.

The mathematical distinction of the present study is the simultaneous treatment of three different objects: the fixed-point set, the polyhedral signature partition, and the directed one-step transition relation. More precisely, for

$$V(S,E,I,R) = \big(S(1-aE-bI),\ E(1+aS-dI),\\ I(1+bS+dE-fR),\ R(1+fI)\big),$$

acting on $S^3 = \{(S,E,I,R) \in \mathbb{R}^4_+ : S+E+I+R = 1\}$, we use the affine signature functions $h_2 = aS-dI, h_3 = bS+dE-fR$. Their sign combinations determine four convex polyhedral regions. We obtain explicit vertex representations of these regions and distinguish geometric facet adjacency from dynamically realizable one-step transitions. In particular, a direct transition may occur between regions that are not facet-adjacent.

The global dynamical result is formulated separately from the local spectral analysis. For every initial state in the interior of the simplex, the iterates converge to a single fixed point of the form

$$(0, E_\infty, 0, 1-E_\infty), \qquad 0 \le E_\infty \le \frac{f}{d+f}.$$

Thus the asymptotic conclusion identifies not only an invariant boundary set but also pointwise convergence of each interior orbit. The signature decomposition additionally describes how trajectories can move between qualitatively distinct regions before approaching their limiting states.

The present results can be compared more specifically with several related studies. Eshmamatova and Tadzhieva [5] investigated the classification of fixed points of operators on simplices. In contrast, the present analysis concerns a specified discrete SEIR operator on S^3 and determines the convex polyhedral partition generated by the two affine signature functions h_2 and h_3.

A discrete SIRD model based on Lotka-Volterra mappings was investigated in [6]. The model considered here includes an explicit exposed class E and combines a signature-based analysis of one-step transitions with a global pointwise convergence result for interior trajectories.

Ganikhodzhaev et al. [7] studied degenerate discrete Lotka-Volterra dynamical systems and their epidemiological applications. The present work focuses on the specified SEIR interaction structure and provides explicit vertex representations, geometric intersections, and directed transition restrictions for its four signature regions.

Related studies of quadratic operators on simplices provide a broader framework for fixed-point and dynamical analysis [11, 12]. The qualitative theory of Lotka-Volterra systems also offers important background for connecting local and global behavior [13].

A more precise comparison with the existing literature further clarifies the scope of our results. Ganikhodzhaev et al. [7] investigated degenerate discrete Lotka-Volterra mappings, establishing results on limit-point sets and invariant curves. Shoyimardonov and Rozikov [11] studied fixed-point structures and global dynamics for a different class of quadratic operators, including a two-dimensional case. Saburov [12] established results concerning surjectivity and bijectivity of quadratic stochastic operators on simplices. These results address different operator classes or different dynamical properties and do not directly provide the explicit directed one-step transition classification obtained here. Our convergence result is specific to the SEIR-type operator under consideration, while the additional signature analysis determines which transitions between its four polyhedral regions are dynamically realizable or impossible.

Thus, the contribution of the present study is not the introduction of the simplex or the Lotka-Volterra formalism itself, but the combination, for the specified discrete SEIR operator, of an explicit polyhedral signature decomposition, an analysis of directed one-step transitions, and a global pointwise convergence theorem.

For the convenience of the reader, we recall several basic definitions related to discrete dynamical systems [14, 15, 16, 17].

Definition 1. A *fixed point* of a discrete dynamical operator V is a point x in the phase space such that $V(x) = x$; that is, a point which remains invariant under the action of the operator.

Definition 2. An *attractor* of a discrete dynamical system $x_{n+1} = V(x_n)$ is a compact invariant set A for which there exists a neighborhood U of A such that $\lim_{n\to\infty} \operatorname{dist}(V^n(x), A) = 0 \quad$ for all $x \in U$. If a fixed point satisfies this property, it is called an *attracting fixed point*.

Definition 3. A *repeller* is an invariant set of a discrete dynamical system for which there exists a neighborhood U such that trajectories starting in $U \setminus A$ move away from A as $n \to \infty$. A fixed point with this property is called a *repelling fixed point*.

Based on these definitions, we proceed to the construction and analysis of the discrete *SEIR* model and investigate the qualitative properties of the corresponding Lotka-Volterra operator V.

SEIR Model

We define the three-dimensional simplex S^3 by

$$S^3 = \left\{ x = (S,E,I,R) \in \mathbb{R}^4 : \; x_i \geq 0, \; \sum_{i=1}^{4} x_i = 1 \right\}$$

On the simplex S^3, we consider a Lotka-Volterra type dynamical system [18] $V : S^3 \to S^3$ that incorporates the latent class of infected individuals. The corresponding discrete SEIR model is given by

$$\begin{aligned} S^{(n+1)} &= S^{(n)}\left(1 - aE^{(n)} - bI^{(n)}\right), \\ E^{(n+1)} &= E^{(n)}\left(1 + aS^{(n)} - dI^{(n)}\right), \\ I^{(n+1)} &= I^{(n)}\left(1 + bS^{(n)} + dE^{(n)} - fR^{(n)}\right), \\ R^{(n+1)} &= R^{(n)}\left(1 + fI^{(n)}\right). \end{aligned} \tag{1}$$

where $0 < a, b, d, f \leq 1$ describe transmission, progression, and recovery interactions.

System (1) can be written in the general Lotka-Volterra form $x_i' = x_i\left(1 + \sum_{j=1}^{4} a_{ij}x_j\right)$, where the interaction matrix has the form

$$A = \begin{pmatrix} 0 & -a & -b & 0 \\ a & 0 & -d & 0 \\ b & d & 0 & -f \\ 0 & 0 & f & 0 \end{pmatrix}.$$

The matrix A induces a partially oriented interaction graph on the set of vertices $\{S, E, I, R\}$.

The variables have the following epidemiological interpretation:

- S — susceptible (healthy) individuals;
- E — infected individuals in the incubation (latent) period;
- I — infectious individuals capable of transmitting the disease;
- R — recovered individuals with immunity.

From the epidemiological point of view, the parameters of system (1) describe pairwise interactions between population compartments.

The coefficient a characterizes the interaction between susceptible and exposed individuals, while b characterizes the interaction between susceptible and infectious individuals. The coefficient d describes the interaction between the exposed and infectious compartments, and f describes the interaction between the infectious and recovered compartments. These coefficients should not be interpreted as conventional constant transition rates of a standard SEIR model.

Indeed, the corresponding interaction terms are aSE, bSI, dEI, and fRI. In particular, the progression-related term dEI depends on the existing infectious population, whereas the recovery-related term fRI depends on the existing recovered population.

The model contains the formal transfer pathways $S \to E \to I \to R$ and $S \to I \to R$. However, unlike the standard SEIR model, the transfers $E \to I$ and $I \to R$ are governed by nonlinear interaction terms rather than linear progression and recovery terms.

Lemma 4. *The operator $V : S^3 \to S^3$ defined by system (1) maps the simplex S^3 into itself.*

Table 1 – Interpretation of the model parameters

Parameter	Interpretation
a	Interaction coefficient between susceptible and exposed individuals.
b	Interaction coefficient between susceptible and infectious individuals.
d	Interaction coefficient governing the nonlinear transfer from E to I.
f	Interaction coefficient governing the nonlinear transfer from I to R.

Proof. Let $x = (S,E,I,R) \in S^3$, i.e.

$$S,E,I,R \geq 0, \qquad S+E+I+R = 1.$$

From system (1) we have

$$\begin{cases} S' &= S(1-aE-bI), \\ E' &= E(1+aS-dI), \\ I' &= I(1+bS+dE-fR), \\ R' &= R(1+fI). \end{cases}$$

Since $0 < a,b,d,f \leq 1$ and $S,E,I,R \geq 0$ with $S+E+I+R = 1$, we have

$$1-aE-bI \geq 1-E-I \geq 0,$$

$$1+aS-dI \geq 1-dI \geq 0,$$

and

$$1+bS+dE-fR \geq 1-fR \geq 0.$$

Moreover, $1+fI > 0$. Hence $S',E',I',R' \geq 0$.

Summing these expressions yields

$$\begin{aligned} S'+E'+I'+R' = S+E+I+R+(-aSE-bSI) \\ +(aSE-dEI)+(bSI+dEI-fRI)+(fRI). \end{aligned}$$

All quadratic terms cancel pairwise, hence $S'+E'+I'+R' = S+E+I+R = 1$. Therefore the simplex S^3 is invariant under the operator V.

Relation with epidemiological data

The parameters of system (1) may be related to epidemiological characteristics of infectious diseases. However, their interpretation differs from that of the transition rates in a standard SEIR model.

Indeed, the changes in the exposed, infectious, and recovered compartments are given by

$$\begin{aligned} E'-E &= aSE-dEI, \\ I'-I &= bSI+dEI-fRI, \\ R'-R &= fRI. \end{aligned}$$

Thus, the transfer from the exposed compartment to the infectious compartment is represented by the interaction term dEI, whereas the transfer from the infectious compartment to the recovered compartment is represented by fRI.

Consequently, the coefficients d and f cannot, in general, be identified directly with the reciprocals of the mean incubation and infectious periods, respectively.

The coefficients a and b describe two infection pathways: transmission leading to the exposed compartment and direct transmission to the infectious compartment, respectively.

Since the model is formulated as a normalized discrete Lotka-Volterra operator, the parameters a,b,d,f are dimensionless interaction coefficients satisfying $0 < a,b,d,f \leq 1$.

Their relationship with epidemiological data requires an appropriate choice of the discrete time step and a calibration procedure consistent with the nonlinear interaction terms.

An important structural feature of the model is that the coordinate hyperplanes are invariant. In particular, if $I = 0$, then $I' = 0$, so the exposed compartment cannot generate infectious individuals in the absence of an existing infectious population. Similarly, if $R = 0$, then $R' = 0$, and recovery cannot create a positive recovered population from zero.

Moreover, the model admits boundary equilibria with $E > 0$ and $I = 0$. These properties distinguish the present Lotka-Volterra formulation from standard SEIR models with linear progression and recovery terms.

In particular, boundary equilibria of the form $(0, E_\infty, 0, 1-E_\infty)$ with $E_\infty > 0$ are mathematically admissible states of the proposed operator. Their existence does not imply that persistent latent infection without infectious individuals necessarily occurs in a real epidemic. Such an epidemiological interpretation would require additional biological assumptions and disease-specific validation.

Therefore, the model is interpreted as a phenomenological discrete dynamical system for investigating qualitative epidemic interactions rather than as a directly calibrated standard SEIR model.

Local infectious thresholds are derived below from the Jacobian spectrum. Disease-specific parameter estimation and validation using epidemiological observations are left for future research.

Jacobian Matrix and Stability Analysis

The dynamical operator V possesses boundary fixed points of the form $M = \left(\frac{f}{b+f}, 0, 0, \frac{b}{b+f}\right), N = \left(0, \frac{f}{d+f}, 0, \frac{d}{d+f}\right)$.

Following the geometric approach in [11, 13], define

$$P = \{x \in S^3 : (Ax)_i \geq 0, \quad i = 1, \ldots, 4\},$$

$$Q = \{x \in S^3 : (Ax)_i \leq 0, \quad i = 1, \ldots, 4\}.$$

For the present operator,

$$Ax = (-aE - bI,\ aS - dI,\ bS + dE - fR,\ fI)^T.$$

To determine P, suppose that $Ax \geq 0$. Since $-aE - bI \geq 0$ and $a, b > 0$, we obtain $E = I = 0$. Thus $S + R = 1$, and the remaining nontrivial inequality is $bS - fR \geq 0$. Hence $S \geq \frac{f}{b+f}$, and therefore $P = [e_1, M]$, $M = \left(\frac{f}{b+f}, 0, 0, \frac{b}{b+f}\right)$. Equivalently,

$$P = \left\{ \left(\frac{f + (1-\lambda)b}{b+f}, 0, 0, \frac{\lambda b}{b+f} \right) : 0 \leq \lambda \leq 1 \right\}.$$

Similarly, let $Ax \leq 0$. The inequality $fI \leq 0$ gives $I = 0$, and then $aS - dI \leq 0$ implies $S = 0$. Consequently, $E + R = 1$ and $dE - fR \leq 0$, so $E \leq \frac{f}{d+f}$. Thus $Q = [N, e_4]$, $N = \left(0, \frac{f}{d+f}, 0, \frac{d}{d+f}\right)$, or, equivalently,

$$Q = \left\{ \left(0, \frac{(1-\lambda)f}{d+f}, 0, \frac{d + \lambda f}{d+f} \right) : 0 \leq \lambda \leq 1 \right\}.$$

Lemma 5. *Every point of the boundary sets P and Q is a fixed point of the dynamical operator V.*

Proof. Consider a point of the set P, where $E = I = 0$ and $S + R = 1$. Substituting these values into system (1), we obtain

$$S' = S, \qquad E' = 0, \qquad I' = 0, \qquad R' = R.$$

Hence $V(x) = x$, and therefore every point of P is a fixed point.

Similarly, for points of the set Q we have $S = I = 0$ and $E + R = 1$. Substituting into system (1) again yields

$$S' = 0, \qquad E' = E, \qquad I' = 0, \qquad R' = R,$$

which implies $V(x) = x$. Therefore every point of Q is also a fixed point. □

Proposition 6. *The complete fixed-point set of the operator V is*

$$\mathrm{Fix}(V) = [e_1, e_4] \cup [e_2, e_4] \cup \{e_3\}.$$

In particular, $P \subset [e_1, e_4]$ and $Q \subset [e_2, e_4]$ are distinguished subsegments of the fixed-point set.

Proof. Let $x = (S, E, I, R) \in S^3$ satisfy $V(x) = x$. Then

$$aSE + bSI = 0, \qquad aSE - dEI = 0,$$

$$bSI + dEI - fRI = 0, \qquad fRI = 0.$$

Since $a, b, d, f > 0$ and all coordinates are nonnegative, the first equality gives $SE = SI = 0$, and the last equality gives $RI = 0$. The second equality then implies $EI = 0$.

If $I > 0$, we obtain $S = E = R = 0$, hence $x = e_3$. If $I = 0$, the remaining condition is $SE = 0$. Thus either $E = 0$, giving $x \in [e_1, e_4]$, or $S = 0$, giving $x \in [e_2, e_4]$.

Conversely, direct substitution into system (1) shows that every point of these two segments, as well as e_3, is fixed. □

Remark 7. The fixed-point structure reflects an important difference between the present Lotka-Volterra operator and the classical SEIR model.

In the present system, the transfer from the exposed compartment to the infectious compartment is governed by the nonlinear interaction term dEI, while the transfer from the infectious compartment to the recovered compartment is governed by fRI.

Consequently, the boundary sets $\{I = 0\}$ and $\{R = 0\}$ are invariant. In particular, if $I = 0$ initially, the model cannot generate an infectious population through progression from E. Likewise, if $R = 0$ initially, the recovered compartment remains empty.

Moreover, the segments $\{(S,0,0,R) : S+R = 1\}$ and $\{(0,E,0,R) : E+R = 1\}$ consist entirely of fixed points. Thus, equilibria with a positive exposed fraction and zero infectious fraction are mathematically admissible.

These properties are consequences of the multiplicative Lotka-Volterra structure and should not be interpreted as standard epidemiological progression and recovery mechanisms. The present model is therefore studied as a qualitative interaction-based SEIR-type system rather than as a conventional compartmental SEIR model.

Theorem 8. *Let $x^{(0)} = (S_0,E_0,I_0,R_0) \in \operatorname{int} S^3$. Then the trajectory generated by the operator V converges to a single fixed point of the segment Q. More precisely, there exists $E_\infty \in \left[0, \frac{f}{d+f}\right]$ such that*

$$\lim_{n\to\infty} V^n(x^{(0)}) = (0,E_\infty,0,1-E_\infty) \in Q.$$

Proof. From system (1), $S_{n+1} \le S_n$, $R_{n+1} \ge R_n$. Since both sequences are bounded, there exist limits $S_n \to S_\infty$ and $R_n \to R_\infty$.

Furthermore, $R_{n+1} - R_n = fR_nI_n \to 0$. Since $R_n \ge R_0 > 0$, it follows that $I_n \to 0$. Also, $S_n - S_{n+1} = S_n(aE_n + bI_n) \to 0$. Suppose that $S_\infty > 0$. Then $E_n \to 0$. However, $\frac{E_{n+1}}{E_n} = 1 + aS_n - dI_n \longrightarrow 1 + aS_\infty > 1$, which contradicts $E_n \to 0$. Hence $S_\infty = 0$.

Since $S_n + E_n + I_n + R_n = 1$, we obtain $E_n \to E_\infty = 1 - R_\infty$. Finally, $\frac{I_{n+1}}{I_n} = 1 + bS_n + dE_n - fR_n$. Since $\frac{I_{n+1}}{I_n} = 1 + bS_n + dE_n - fR_n \longrightarrow 1 + dE_\infty - fR_\infty$, suppose, by contradiction, that $dE_\infty - fR_\infty > 0$. Then there exist $\varepsilon > 0$ and n_0 such that $\frac{I_{n+1}}{I_n} > 1 + \varepsilon$ for all $n \ge n_0$, which contradicts $I_n \to 0$.

Therefore $dE_\infty - fR_\infty \le 0$. Together with $E_\infty + R_\infty = 1$, this gives $E_\infty \le \frac{f}{d+f}$. Thus

$$\lim_{n\to\infty} V^n(x^{(0)}) = (0,E_\infty,0,1-E_\infty) \in Q.$$

□

The graphical representation of the sets P and Q in the simplex is shown in Figure 1. The sets

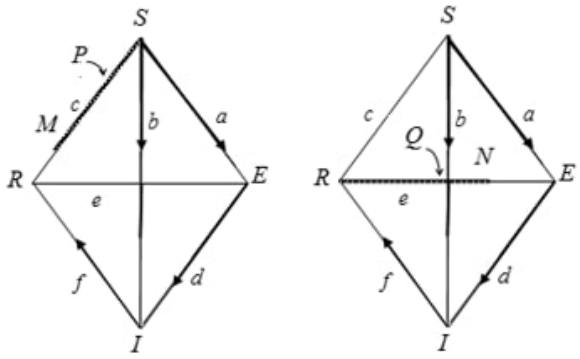


Figure 1 - Graphical representation of the sets P and Q in the simplex.

P and Q are distinguished boundary segments consisting entirely of fixed points of the discrete SEIR Lotka-Volterra operator. The segment P contains states with $E = I = 0$, whereas the segment Q contains states with $S = I = 0$ and may include a positive exposed fraction.

To investigate the local stability properties of these fixed points, we perform a spectral analysis of the Jacobian matrix associated with the model.

Let us analyze the local stability of the fixed points of the operator $V : S^3 \to S^3$ corresponding to system (1).

The Jacobian matrix of the mapping V is defined by $J(x) = \left(\frac{\partial V_i}{\partial x_j}\right)$.

For the system (1) we obtain

$$J(x) = \begin{pmatrix} 1-aE-bI & -aS & -bS & 0 \\ aE & 1+aS-dI & -dE & 0 \\ bI & dI & 1+bS+dE-fR & -fI \\ 0 & 0 & fR & 1+fI \end{pmatrix}$$

We first consider the fixed point $M = \left(\frac{f}{b+f}, 0, 0, \frac{b}{b+f}\right)$.

Substituting these coordinates into the Jacobian matrix, we obtain

$$J(M) = \begin{pmatrix} 1 & -\frac{af}{b+f} & -\frac{bf}{b+f} & 0 \\ 0 & 1+\frac{af}{b+f} & 0 & 0 \\ 0 & 0 & 1 & 0 \\ 0 & 0 & \frac{fb}{b+f} & 1 \end{pmatrix}.$$

The characteristic polynomial of this matrix is $(1-\lambda)^3\left(1+\frac{af}{b+f}-\lambda\right)$.

Hence the eigenvalues are $\lambda_1 = \lambda_2 = \lambda_3 = 1$, $\lambda_4 = 1+\frac{af}{b+f} > 1$.

Since $\lambda_4 > 1$, the fixed point M is unstable. Notice that the remaining three eigenvalues are equal to one; hence M is nonhyperbolic. Therefore, the linearization establishes instability in the direction corresponding to λ_4, but does not by itself imply that M is a repeller in all directions.

Next we consider the fixed point $N = \left(0, \frac{f}{d+f}, 0, \frac{d}{d+f}\right)$.

Substituting these coordinates into the Jacobian matrix, we obtain

$$J(N) = \begin{pmatrix} 1-\frac{af}{d+f} & 0 & 0 & 0 \\ \frac{af}{d+f} & 1 & -\frac{df}{d+f} & 0 \\ 0 & 0 & 1 & 0 \\ 0 & 0 & \frac{fd}{d+f} & 1 \end{pmatrix}.$$

The characteristic polynomial has the form $(1-\lambda)^3\left(1-\frac{af}{d+f}-\lambda\right)$.

Therefore the eigenvalues are $\lambda_1 = \lambda_2 = \lambda_3 = 1$, $\lambda_4 = 1-\frac{af}{d+f} < 1$.

Since $\lambda_4 < 1$ while $\lambda_1 = \lambda_2 = \lambda_3 = 1$, the fixed point N is nonhyperbolic. The eigenvalue $\lambda_4 < 1$ indicates contraction in the corresponding transverse direction. However, linearization alone does not imply asymptotic stability of N. The forward convergence established above shows instead that interior trajectories converge to the fixed segment Q, which contains N.

Remark 9. Both M and N are nonhyperbolic fixed points. The full Jacobian matrices possess three unit eigenvalues, and the dynamics restricted to the simplex also have unit multipliers. Therefore, linearization alone does not determine the complete local stability of these fixed points. At M, the eigenvalue greater than one proves instability in at least one direction, whereas at N the eigenvalue less than one indicates contraction in one direction. The global forward behavior is determined by the convergence theorem above, which shows that every interior trajectory converges to a point of the fixed segment Q.

Finally, in order to determine the trajectory routes of the dynamical system on the simplex corresponding to the regions induced by sign structures, we introduce the notion of signatures.

Interaction graph and acyclic structure

The interaction matrix A induces the directed graph $S \to E \to I \to R$ together with the additional edge $S \to I$.

This graph does not contain directed cycles and therefore it is an acyclic partially oriented graph.

Lemma 10. *The interaction graph generated by the matrix A is acyclic.*

Proof. From the definition of the coefficients a_{ij} we obtain the edges

$$S \to E, \quad S \to I, \quad E \to I, \quad I \to R.$$

These edges form the directed chain

$$S \to E \to I \to R.$$

Since there is no edge leading from R back to the preceding vertices, the graph does not contain directed cycles. □

Signature partition

Definition 11. Let x be an interior point of the simplex. The ordered tuple

$$\delta(x) = \big(\operatorname{sgn}(x_1' - x_1), \ldots, \operatorname{sgn}(x_4' - x_4)\big)$$

is called the signature of x, provided that all coordinate increments are nonzero.

A positive sign indicates an increase of the corresponding coordinate under one iteration,

whereas a negative sign indicates a decrease. The closures of the regions determined by these strict sign conditions will be called closed signature regions.

Consider the discrete Lotka-Volterra-type SEIR operator

$$\begin{cases} S' &= S(1-aE-bI), \\ E' &= E(1+aS-dI), \\ I' &= I(1+bS+dE-fR), \\ R' &= R(1+fI), \end{cases}$$

where $a,b,d,f>0$ and $S^3=\{(S,E,I,R)\in\mathbb{R}^4_+ : S+E+I+R=1\}$. We assume that the parameters are chosen so that $V(S^3)\subseteq S^3$.

The coordinate increments satisfy

$$\begin{cases} S'-S &= Sh_1(x), \\ E'-E &= Eh_2(x), \\ I'-I &= Ih_3(x), \\ R'-R &= Rh_4(x), \end{cases}$$

where

$$\begin{cases} h_1(x) &= -aE-bI, \\ h_2(x) &= aS-dI, \\ h_3(x) &= bS+dE-fR, \\ h_4(x) &= fI. \end{cases}$$

For every interior point of S^3, we have $h_1(x)<0$ and $h_4(x)>0$. Consequently, only the signs of h_2 and h_3 may vary.

The four possible interior signatures are

$$\delta_1=(-++{+}),\quad \delta_2=(--{+}{+}),$$
$$\delta_3=(-+-{+}),\quad \delta_4=(---{+}).$$

The corresponding closed signature regions are defined by

$$F_1=\{x\in S^3 : h_2(x)\geq 0,\ h_3(x)\geq 0\},$$
$$F_2=\{x\in S^3 : h_2(x)\leq 0,\ h_3(x)\geq 0\},$$
$$F_3=\{x\in S^3 : h_2(x)\geq 0,\ h_3(x)\leq 0\},$$
$$F_4=\{x\in S^3 : h_2(x)\leq 0,\ h_3(x)\leq 0\}.$$

Equivalently,

$$F_1=\{x\in S^3 : aS-dI\geq 0,\ bS+dE-fR\geq 0\},$$
$$F_2=\{x\in S^3 : aS-dI\leq 0,\ bS+dE-fR\geq 0\},$$
$$F_3=\{x\in S^3 : aS-dI\geq 0,\ bS+dE-fR\leq 0\},$$
$$F_4=\{x\in S^3 : aS-dI\leq 0,\ bS+dE-fR\leq 0\}.$$

The separating hyperplanes are

$$H_2=\{x\in S^3 : aS-dI=0\}$$

and

$$H_3=\{x\in S^3 : bS+dE-fR=0\}.$$

Proposition 12. *Let* $L=\left(\frac{d}{a+d},0,\frac{a}{a+d},0\right)$, $M=\left(\frac{f}{b+f},0,0,\frac{b}{b+f}\right)$, $N=\left(0,\frac{f}{d+f},0,\frac{d}{d+f}\right)$, *and* $C=\left(\frac{df}{D},0,\frac{af}{D},\frac{bd}{D}\right)$, $D=df+af+bd$.

Then the closed signature regions have the convex-hull representations $F_1=\mathrm{co}\{e_1,e_2,L,M,N,C\}$, $F_2=\mathrm{co}\{e_2,e_3,L,N,C\}$, $F_3=\mathrm{co}\{e_4,M,N,C\}$, *and* $F_4=\mathrm{co}\{e_3,e_4,N,C\}$.

Moreover, $H_2\cap H_3=[N,C]$.

Proof. We first provide a detailed construction of F_1 using its defining inequalities.

Consider the signature $\delta_1=(-++{+})$. The corresponding system of inequalities is

$$\begin{cases} -aE-bI\leq 0, \\ aS-dI\geq 0, \\ bS+dE-fR\geq 0, \\ fI\geq 0, \\ S+E+I+R=1, \\ S,E,I,R\geq 0. \end{cases}$$

Since $a,b,d,f>0$, the first and fourth inequalities are automatically satisfied. Therefore,

$$F_1=\left\{x\in S^3 : aS-dI\geq 0,\ bS+dE-fR\geq 0\right\}.$$

We determine the boundary vertices of F_1 by solving the inequalities on the edges and faces of the simplex.

Case 1. The edge $[e_1,e_3]$.

Set $E=R=0$. Then $S+I=1$, and $aS-dI\geq 0$. Substituting $I=1-S$, we obtain $aS-d(1-S)\geq 0$, $(a+d)S\geq d$. Consequently,

$$\frac{d}{a+d}\leq S\leq 1, \qquad 0\leq I\leq \frac{a}{a+d}.$$

The separating point is $L=\left(\frac{d}{a+d},0,\frac{a}{a+d},0\right)$.

On this edge, the second inequality is $bS\geq 0$ and is automatically satisfied. Thus the admissible segment is $[L,e_1]$.

Case 2. The edge $[e_1,e_4]$.

Set $E=I=0$. Then $S+R=1$, and $bS-fR\geq 0$. Substituting $R=1-S$, we get $bS-f(1-S)\geq 0$, $(b+f)S\geq f$. Hence

$$\frac{f}{b+f}\leq S\leq 1, \qquad 0\leq R\leq \frac{b}{b+f}.$$

The separating point is $M=\left(\frac{f}{b+f},0,0,\frac{b}{b+f}\right)$.

The first inequality reduces to $aS\geq 0$, so the admissible segment is $[M,e_1]$.

Case 3. The edge $[e_2,e_4]$.

Set $S=I=0$. Then $E+R=1$, and $dE-fR\geq 0$. Substituting $R=1-E$, we obtain $dE-f(1-E)\geq 0$, $(d+f)E\geq f$. Thus

$$\frac{f}{d+f}\leq E\leq 1, \qquad 0\leq R\leq \frac{d}{d+f}.$$

The separating point is $N=\left(0,\frac{f}{d+f},0,\frac{d}{d+f}\right)$.

Since $aS-dI=0$ on this edge, the admissible segment is $[N,e_2]$.

Case 4. Intersection of the separating hyperplanes on $E=0$.

Set $E=0$ and solve

$$\begin{cases} aS-dI=0,\\ bS-fR=0,\\ S+I+R=1. \end{cases}$$

From the first two equations, $I=\frac{a}{d}S, R=\frac{b}{f}S$. Substituting into the simplex equation, $S+\frac{a}{d}S+\frac{b}{f}S=1$. Multiplying by df gives $(df+af+bd)S=df$. Let $D=df+af+bd$. Then

$$S=\frac{df}{D}, \qquad I=\frac{af}{D}, \qquad R=\frac{bd}{D}.$$

Therefore, $C=\left(\frac{df}{D},0,\frac{af}{D},\frac{bd}{D}\right)$.

Completeness of the vertex set.

The four simplex vertices satisfy

	h_2	h_3
e_1	a	b
e_2	0	d
e_3	$-d$	0
e_4	0	$-f$

Hence $e_1,e_2\in F_1$, whereas $e_3,e_4\notin F_1$.

A vertex of F_1 must be determined by three independent active constraints among the four coordinate boundaries and the two separating hyperplanes.

The intersections with one separating hyperplane and two coordinate boundaries produce the points L, M, and N, apart from simplex vertices.

The intersection of both separating hyperplanes with $E=0$ produces C, while the intersection with $S=0$ or $I=0$ produces N. No additional vertices arise.

Consequently, the complete vertex set of F_1 is

$$\mathrm{Vert}(F_1)=\{e_1,e_2,L,M,N,C\}.$$

Since F_1 is a bounded intersection of closed half-spaces, it is the convex hull of its vertices. Therefore,

$$F_1=\mathrm{co}\{e_1,e_2,L,M,N,C\}.$$

The remaining signature regions are determined analogously by solving their corresponding systems of linear inequalities on the simplex.

More precisely, the same procedure, based on the intersections of the separating hyperplanes with the edges and faces of the simplex, yields

$$\mathrm{Vert}(F_2)=\{e_2,e_3,L,N,C\},$$
$$\mathrm{Vert}(F_3)=\{e_4,M,N,C\},$$
$$\mathrm{Vert}(F_4)=\{e_3,e_4,N,C\}.$$

Furthermore, the intersection of the two separating hyperplanes is determined by $aS=dI, bS+dE=fR$, together with $S+E+I+R=$

$1, S, E, I, R \geq 0$. These equations define a line segment inside the simplex. Its endpoints are obtained by setting $S = 0$ and $E = 0$, respectively, giving N and C. Therefore, $H_2 \cap H_3 = [N, C]$.

Since each F_i is a bounded polyhedron, it coincides with the convex hull of its vertices. This completes the proof. □

Corollary 13. *The four signature regions cover the simplex: $S^3 = F_1 \cup F_2 \cup F_3 \cup F_4$. Their interiors are pairwise disjoint.*

The common facets are

$$F_1 \cap F_2 = \mathrm{co}\{e_2, L, N, C\}, F_1 \cap F_3 = \mathrm{co}\{M, N, C\},$$

$F_2 \cap F_4 = \mathrm{co}\{e_3, N, C\}$, *and* $F_3 \cap F_4 = \mathrm{co}\{e_4, N, C\}$.

The remaining pairwise intersections are

$$F_1 \cap F_4 = [N, C], \qquad F_2 \cap F_3 = [N, C].$$

Hence the complete facet-adjacency relations are

$$F_1 \sim F_2, \qquad F_1 \sim F_3, \qquad F_2 \sim F_4, \qquad F_3 \sim F_4.$$

Proof. The covering and disjoint-interior properties follow directly from the four possible sign combinations of h_2 and h_3.

For example, $F_1 \cap F_2 = \{x \in S^3 : h_2 = 0,\ h_3 \geq 0\}$. Using the vertex characterization established above gives $F_1 \cap F_2 = \mathrm{co}\{e_2, L, N, C\}$.

The other common facets follow analogously from the corresponding equalities and inequalities.

For the opposite pairs, both separating functions must vanish. Therefore,

$$F_1 \cap F_4 = F_2 \cap F_3 = H_2 \cap H_3 = [N, C].$$

These intersections are one-dimensional and hence are not facets of the three-dimensional regions. □

Remark 14. The facet-adjacency relations describe the geometry of the signature partition. They do not imply that a discrete trajectory can move only between facet-adjacent regions.

The admissible one-step transitions under V must be determined separately by examining $h_2(V(x))$ and $h_3(V(x))$ for points in each region.

Epidemiological interpretation of the regions F_i

The polyhedra F_1, F_2, F_3, F_4 obtained from the signature partition admit a natural epidemiological interpretation. Each region corresponds to a specific configuration of increasing or decreasing population fractions (S, E, I, R).

The signs in the signature indicate whether the corresponding compartment increases or decreases along the trajectory of the system. Therefore each polyhedron describes a particular qualitative stage of the epidemic dynamics.

For example, a negative sign in the first coordinate indicates a decrease in the susceptible population due to infection spread, while positive signs in the other coordinates correspond to the growth of exposed, infectious, or recovered individuals.

Global trajectory structure

The signature partition provides a geometric decomposition of the simplex into four closed convex polyhedra. The facet-adjacency relations are

$$F_1 \sim F_2, \qquad F_1 \sim F_3, \qquad F_2 \sim F_4, \qquad F_3 \sim F_4.$$

However, geometric adjacency and dynamical transitions are different notions.

Since the operator is discrete, a trajectory may cross two separating hyperplanes in a single iteration. Therefore, the actual destination region must be determined by examining both separating functions after applying the operator.

For convenience, introduce $u(x) = aS - dI, v(x) = bS + dE - fR$, and $A(x) = aE + bI$.

The four signature regions correspond to

	u	v
F_1	≥ 0	≥ 0
F_2	≤ 0	≥ 0
F_3	≥ 0	≤ 0
F_4	≤ 0	≤ 0

Proposition 15. *For every $x = (S, E, I, R) \in S^3$, the separating functions satisfy $u(V(x)) = u - aSA - dIv$ and $v(V(x)) = v - bSA + dEu - f^2RI$.*

Proof. The first and third coordinates of the operator are $S' = S(1-A), I' = I(1+v)$. Consequently,

$$\begin{aligned} u(V(x)) &= aS' - dI' = aS(1-A) - dI(1+v) \\ &= aS - dI - aSA - dIv = u - aSA - dIv. \end{aligned}$$

Similarly, $E' = E(1+u), R' = R(1+fI)$. Therefore,

$$\begin{aligned} v(V(x)) &= bS' + dE' - fR' \\ &= bS(1-A) + dE(1+u) \\ &\quad - fR(1+fI) = bS + dE - fR \\ &\quad - bSA + dEu - f^2RI \\ &= v - bSA + dEu - f^2RI. \end{aligned}$$

The identities follow. □

Proposition 16. *The following one-step restrictions hold: $V(F_2) \subseteq F_2 \cup F_4$, and $V(F_4) \subseteq F_3 \cup F_4$.*

Proof. Let $x \in F_2$. Then $u \le 0, v \ge 0$. Since all parameters and coordinates are nonnegative, $u(V(x)) = u - aSA - dIv \le 0$. Thus the image cannot have a positive first separating function. It follows that $V(x) \in F_2 \cup F_4$.

Now let $x \in F_4$. Then $u \le 0, v \le 0$. Hence $v(V(x)) = v - bSA + dEu - f^2RI \le 0$. Therefore, $V(x) \in F_3 \cup F_4$. This proves both restrictions. □

Corollary 17. *For points belonging to the strict signature regions, the one-step transitions*

$$F_2 \to F_1, \qquad F_2 \to F_3, \qquad F_4 \to F_1, \qquad F_4 \to F_2$$

are impossible.

Proof. The assertion follows directly from Proposition 16. Indeed, the first inclusion prevents an image of F_2 from entering the strict regions F_1 or F_3, while the second inclusion prevents an image of F_4 from entering the strict regions F_1 or F_2. □

We now apply the successive-iteration method to each common facet. Following the geometric construction of the signature regions, an arbitrary point of a common facet is represented as a convex combination of its vertices.

Proposition 18. *On the common facet $F_1 \cap F_2$, the image satisfies $u(V(x)) \le 0$. Its destination is determined by the sign of $v(V(x))$.*

Proof. The common facet is $F_1 \cap F_2 = \mathrm{co}\{e_2, L, N, C\}$. Let $x = \alpha_1 e_2 + \alpha_2 L + \alpha_3 N + \alpha_4 C$, where $\alpha_i \ge 0, \sum_{i=1}^4 \alpha_i = 1$.

Using the coordinates of the vertices, we obtain

$$\begin{aligned} S &= \frac{d\alpha_2}{a+d} + \frac{df\alpha_4}{D}, E = \alpha_1 + \frac{f\alpha_3}{d+f}, \\ I &= \frac{a\alpha_2}{a+d} + \frac{af\alpha_4}{D}, R = \frac{d\alpha_3}{d+f} + \frac{bd\alpha_4}{D}, \end{aligned}$$

where $D = df + af + bd$.

Substituting into the first separating function gives

$$\begin{aligned} u = aS - dI = a\left(\frac{d\alpha_2}{a+d} + \frac{df\alpha_4}{D}\right) \\ - d\left(\frac{a\alpha_2}{a+d} + \frac{af\alpha_4}{D}\right) = 0. \end{aligned}$$

For the second separating function,

$$v = bS + dE - fR = d\alpha_1 + \frac{bd}{a+d}\alpha_2 \ge 0.$$

Thus every point of the facet satisfies $u = 0, v \ge 0$.

The first iteration of the exposed coordinate is $E' = E(1+u) = E$.

At the second iteration, $E'' = E'(1+u(V(x)))$. We compute

$$u(V(x)) = aS' - dI' = aS(1-A) - dI(1+v).$$

Since $aS = dI$ on the facet,

$$u(V(x)) = aS[(1-A) - (1+v)] = -aS(A+v).$$

In terms of the barycentric coefficients,

$$\begin{aligned} u(V(x)) = &-a\left(\frac{d\alpha_2}{a+d} + \frac{df\alpha_4}{D}\right) \\ &\times \left[d\alpha_1 + \frac{bd\alpha_2}{a+d} + a\left(\alpha_1 + \frac{f\alpha_3}{d+f}\right)\right. \\ &\left. + b\left(\frac{a\alpha_2}{a+d} + \frac{af\alpha_4}{D}\right)\right] \le 0. \end{aligned}$$

Therefore, $E'' - E' = E'u(V(x)) \le 0$.

This establishes the direction toward the nonpositive side of H_2.

To identify the destination region, we must also evaluate $v(V(x)) = v - bSA - f^2RI$.

Hence

$$\begin{cases} v(V(x)) \ge 0 & \Longrightarrow V(x) \in F_2, \\ v(V(x)) \le 0 & \Longrightarrow V(x) \in F_4. \end{cases}$$

In the equality case, the image may belong to both closed regions.

Thus the crossing of H_2 is one-sided on this facet, but the destination is not necessarily F_2. □

Proposition 19. *The common facet $F_2 \cap F_4$ satisfies $V(F_2 \cap F_4) \subseteq F_4$.*

Proof. We have $F_2 \cap F_4 = \mathrm{co}\{e_3, N, C\}$.

Let $x = \alpha_1 e_3 + \alpha_2 N + \alpha_3 C$, where $\alpha_i \ge 0, \alpha_1 + \alpha_2 + \alpha_3 = 1$.

The coordinates are

$$S = \frac{df\alpha_3}{D}, E = \frac{f\alpha_2}{d+f},$$
$$I = \alpha_1 + \frac{af\alpha_3}{D}, R = \frac{d\alpha_2}{d+f} + \frac{bd\alpha_3}{D}.$$

Substitution gives

$$u = aS - dI = \frac{adf\alpha_3}{D} - d\alpha_1 - \frac{adf\alpha_3}{D} = -d\alpha_1 \le 0,$$

and

$$v = bS + dE - fR = \frac{bdf\alpha_3}{D} + \frac{df\alpha_2}{d+f} - \frac{df\alpha_2}{d+f} - \frac{bdf\alpha_3}{D} = 0.$$

The first iteration of the infectious coordinate satisfies $I' = I(1+v) = I$.

For the second iteration, $I'' = I'(1 + v(V(x)))$.

Using Proposition 15,

$$v(V(x)) = v - bSA + dEu - f^2RI = -bSA - d^2E\alpha_1 - f^2RI.$$

Each term on the right-hand side is nonpositive. Therefore, $v(V(x)) \le 0$, and consequently $I'' \le I'$.

The other separating function is

$$u(V(x)) = u - aSA - dIv = -d\alpha_1 - aSA \le 0.$$

Thus both required inequalities hold: $u(V(x)) \le 0, v(V(x)) \le 0$. Hence $V(x) \in F_4$ for every $x \in F_2 \cap F_4$. □

Proposition 20. *On the common facet $F_1 \cap F_3$, the direction of the image depends on the parameters and barycentric coefficients.*

Proof. The common facet is $F_1 \cap F_3 = \mathrm{co}\{M, N, C\}$. Let $x = \alpha_1 M + \alpha_2 N + \alpha_3 C$, where $\alpha_i \ge 0, \alpha_1 + \alpha_2 + \alpha_3 = 1$.

Then

$$S = \frac{f\alpha_1}{b+f} + \frac{df\alpha_3}{D}, E = \frac{f\alpha_2}{d+f},$$
$$I = \frac{af\alpha_3}{D}, R = \frac{b\alpha_1}{b+f} + \frac{d\alpha_2}{d+f} + \frac{bd\alpha_3}{D}.$$

We obtain

$$u = aS - dI = \frac{af\alpha_1}{b+f} \ge 0,$$

whereas $v = bS + dE - fR = 0$. Thus $I' = I(1+v) = I$.

At the next iteration, $I'' = I'(1 + v(V(x)))$.

By Proposition 15, $v(V(x)) = -bSA + dEu - f^2RI$.

Substituting $A = aE + bI, u = aS - dI$, gives

$$v(V(x)) = -bS(aE + bI) + dE(aS - dI) - f^2RI = a(d-b)SE - b^2SI - d^2EI - f^2RI.$$

Since $v = 0$, we have $fR = bS + dE$. Therefore, $f^2RI = fI(bS + dE)$.

Consequently,

$$v(V(x)) = a(d-b)SE - I\big[b(b+f)S + d(d+f)E\big].$$

In barycentric coordinates, this is

$$v(V(x)) = a(d-b)\left(\frac{f\alpha_1}{b+f} + \frac{df\alpha_3}{D}\right)\frac{f\alpha_2}{d+f} - \frac{af\alpha_3}{D}\left[b(b+f)\left(\frac{f\alpha_1}{b+f} + \frac{df\alpha_3}{D}\right) + d(d+f)\frac{f\alpha_2}{d+f}\right].$$

If $d \le b$, then $v(V(x)) \le 0$.

Nevertheless, the other separating function must also be examined:

$$u(V(x)) = u - aSA = \frac{af\alpha_1}{b+f} - a\left(\frac{f\alpha_1}{b+f} + \frac{df\alpha_3}{D}\right)\left(\frac{af\alpha_2}{d+f} + \frac{abf\alpha_3}{D}\right).$$

Thus, when $d \le b$,

$$\begin{cases} u(V(x)) \ge 0 & \Longrightarrow V(x) \in F_3, \\ u(V(x)) \le 0 & \Longrightarrow V(x) \in F_4. \end{cases}$$

For $d > b$, the sign of $v(V(x))$ may also vary. The destination must then be determined by both computed expressions.

Hence no unconditional transition $F_1 \to F_3$ follows from facet adjacency alone. □

Proposition 21. *On the common facet $F_3 \cap F_4$, the image belongs to F_3 or F_4, depending on the barycentric coefficients.*

Proof. The common facet is $F_3 \cap F_4 = \mathrm{co}\{e_4, N, C\}$. Let $x = \alpha_1 e_4 + \alpha_2 N + \alpha_3 C$, where $\alpha_i \ge 0, \alpha_1 + \alpha_2 + \alpha_3 = 1$.

Its coordinates are

$$S = \frac{df\alpha_3}{D}, E = \frac{f\alpha_2}{d+f},$$
$$I = \frac{af\alpha_3}{D}, R = \alpha_1 + \frac{d\alpha_2}{d+f} + \frac{bd\alpha_3}{D}.$$

Therefore, $u = aS - dI = 0$, and $v = bS + dE - fR = -f\alpha_1 \le 0$.

The first iteration gives $E' = E(1+u) = E$.

The second iteration is $E'' = E'(1+u(V(x)))$.

We calculate

$$u(V(x)) = u - aSA - dIv = -aSA + dfI\alpha_1.$$

Since $aS = dI$, $u(V(x)) = aS[f\alpha_1 - A]$.

Using

$$A = aE + bI = \frac{af\alpha_2}{d+f} + \frac{abf\alpha_3}{D},$$

we obtain

$$u(V(x)) = aS\left[f\alpha_1 - \frac{af\alpha_2}{d+f} - \frac{abf\alpha_3}{D}\right].$$

Consequently, $E'' - E' = E'u(V(x))$.

The sign of this difference depends on the barycentric coefficients.

The second separating function is

$$v(V(x)) = v - bSA + dEu - f^2RI = -f\alpha_1 - bSA - f^2RI \le 0.$$

Therefore,

$$\begin{cases} u(V(x)) \ge 0 & \Longrightarrow V(x) \in F_3, \\ u(V(x)) \le 0 & \Longrightarrow V(x) \in F_4. \end{cases}$$

For $S > 0$, the first condition is equivalent to

$$\alpha_1 \ge \frac{a\alpha_2}{d+f} + \frac{ab\alpha_3}{D}.$$

The reverse inequality determines the opposite side of H_2.

Thus the local crossing direction depends explicitly on the point of the common facet. □

Proposition 22. *A direct one-step transition from the strict interior of F_1 to the strict interior of F_4 is possible, although these regions are not facet-adjacent.*

Proof. Consider $C = \left(\frac{df}{D}, 0, \frac{af}{D}, \frac{bd}{D}\right)$, $D = df + af + bd$.

At this point, $u(C) = v(C) = 0$. Moreover, $A(C) = bI_C > 0$.

Using Proposition 15,

$$u(V(C)) = -aS_C A(C) = -abS_C I_C < 0.$$

Similarly,

$$v(V(C)) = -bS_C A(C) - f^2 R_C I_C = -b^2 S_C I_C - f^2 R_C I_C < 0.$$

Thus the image of C satisfies both strict inequalities defining the interior signature of F_4.

Since $u \circ V$ and $v \circ V$ are continuous, these strict inequalities persist in a sufficiently small neighborhood of C.

To construct interior points of F_1 approaching C, let $p = \frac{e_1+e_2+e_3+e_4}{4}$, and define

$$x_{\varepsilon,t} = (1 - \varepsilon - t)C + \varepsilon e_1 + tp,$$

where $\varepsilon, t > 0$ and $\varepsilon + t < 1$.

All four coordinates of $x_{\varepsilon,t}$ are positive.

Furthermore, $u(x_{\varepsilon,t}) = \varepsilon a + t\,u(p)$, and $v(x_{\varepsilon,t}) = \varepsilon b + t\,v(p)$.

For sufficiently small positive t relative to ε, both expressions are positive. Hence $x_{\varepsilon,t} \in \operatorname{int} F_1$.

By taking ε and t sufficiently small, continuity gives $u(V(x_{\varepsilon,t})) < 0, v(V(x_{\varepsilon,t})) < 0$.

Therefore, $V(x_{\varepsilon,t}) \in \operatorname{int} F_4$.

This establishes the existence of a direct one-step jump $F_1 \longrightarrow F_4$. □

Remark 23. The preceding results distinguish geometric facet adjacency from one-step dynamical transitions.

The geometric adjacency graph has only four edges:

$$F_1 - F_2, \quad F_1 - F_3, \quad F_2 - F_4, \quad F_3 - F_4.$$

The direct jump $F_1 \to F_4$ does not introduce a new edge into this geometric adjacency graph.

Moreover, the successive-iteration calculations determine local crossing conditions, not global convergence. Global convergence must be justified by an independent theorem.

The geometric structure of the simplex together with the polyhedra F_1, F_2, F_3, F_4 and the boundary sets P and Q is illustrated in Fig. 2.

Corollary 24. *For every initial point $x^{(0)} \in \operatorname{int} S^3$, the forward trajectory converges to a single point of the fixed segment Q. Consequently, $\omega(x^{(0)}) = \{(0, E_\infty, 0, 1 - E_\infty)\} \subset Q$, where $0 \le E_\infty \le \frac{f}{d+f}$.*

The local transition structure between the polyhedra F_1, F_2, F_3, F_4 is illustrated in Fig. 3.

Proposition 25. *For every $0 < a, b, d, f \le 1$, a direct one-step transition from the strict signature region F_3 to the strict signature region F_2 is impossible. Equivalently,*

$$V(\operatorname{int} F_3) \cap \operatorname{int} F_2 = \varnothing,$$

where the interiors are understood relative to the strict signature inequalities.

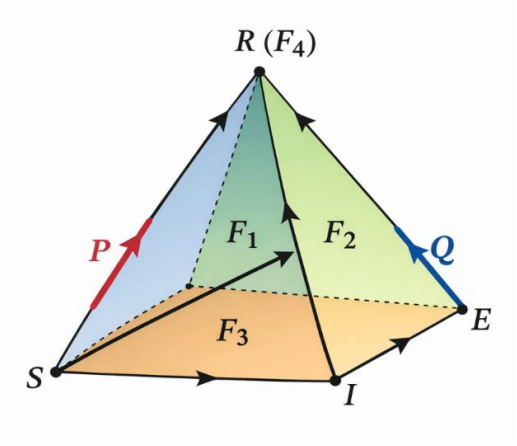


Figure 2 - Geometric representation of the simplex S^3 and the four signature polyhedra F_1, F_2, F_3, F_4 of the discrete SEIR Lotka-Volterra operator. The boundary segments P and Q are distinguished sets consisting entirely of fixed points of the operator. The directed edges indicate the interaction pathways $S \to E \to I \to R$ and $S \to I \to R$.

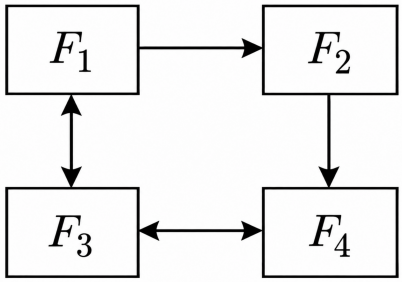


Figure 3 - Schematic representation of local transition directions between the four facet-adjacent signature regions. Single arrows indicate one-sided crossing conditions established on the corresponding common facets. Double arrows indicate facets where the crossing direction may depend on the parameters or the position of the initial point. The diagram does not represent all possible one-step transitions; in particular, a direct jump $F_1 \to F_4$ is possible.

Proof. Put

$$u = aS - dI, v = bS + dE - fR, A = aE + bI.$$

Suppose, to the contrary, that $x \in F_3$ and $V(x) \in F_2$ in the strict signature sense. Then

$$u > 0, v < 0, u' = u(V(x)) < 0, v' = v(V(x)) > 0.$$

The signature identities give

$$u' = aS(1-A) - dI(1+v)$$

and

$$v' = (1+u)v - bS(A+u) + fR(u-fI).$$

Since $v < 0$, $u > 0$, $A \geq 0$, and $S, R \geq 0$, the inequality $v' > 0$ necessarily implies

$$u > fI.$$

Consequently,

$$aS > (d+f)I. \tag{2}$$

On the other hand, $u' < 0$ and $v < 0$ imply

$$aS(1-A) < dI(1+v) < dI.$$

As $S > 0$, we obtain

$$A > 1 - \frac{dI}{aS}.$$

Using (2), it follows that

$$A > 1 - \frac{d}{d+f} = \frac{f}{d+f}. \tag{3}$$

We now derive the opposite bound. Since $v < 0$,

$$bS + dE < fR = f(1-S-E-I),$$

and hence

$$(d+f)E < f - (f+b)S - fI.$$

Therefore,

$$\begin{aligned}(d+f)A &= a(d+f)E + b(d+f)I \\ &< af - a(f+b)S - afI + b(d+f)I.\end{aligned}$$

By (2),

$$a(f+b)S > (f+b)(d+f)I.$$

It follows that

$$\begin{aligned}(d+f)A &< af - (f+b)(d+f)I - afI \\ &\quad + b(d+f)I = af - f(d+f+a)I \leq f,\end{aligned}$$

where the last inequality uses $a \leq 1$ and $I \geq 0$. Thus

$$A < \frac{f}{d+f},$$

contradicting (3).

Hence a strict one-step transition $F_3 \to F_2$ cannot occur. □

Table 2 – Summary of one-step transitions between strict signature regions.

From	To	Status
F_1	F_2	Realizable
F_1	F_3	Realizable
F_1	F_4	Realizable
F_2	F_1	Impossible
F_2	F_3	Impossible
F_2	F_4	Realizable
F_3	F_1	Realizable
F_3	F_2	Impossible
F_3	F_4	Realizable
F_4	F_1	Impossible
F_4	F_2	Impossible
F_4	F_3	Realizable

Summary of directed signature transitions.

The classification of all twelve directed one-step transitions between distinct strict signature regions is now complete. In particular, the transition $F_3 \to F_2$ is impossible by the preceding proposition.

This conclusion follows from the dynamical inequalities of the Lotka-Volterra operator, rather than from geometric non-adjacency. Indeed, non-adjacent signature regions may admit direct one-step transitions, as demonstrated by the realizable transition $F_1 \to F_4$.

Here, "realizable" means that at least one transition between the corresponding strict regions exists for admissible parameters. "Impossible" means that the transition is excluded by the analytical sign constraints.

This classification concerns discrete one-step transitions, not geometric facet adjacency.

Lyapunov-Type Dissipation and Global Convergence

The monotone structure of the recovered component provides a natural Lyapunov-type quantity for the discrete SEIR Lotka-Volterra system.

Define $\mathscr{L}(S,E,I,R) = 1 - R = S + E + I$.

Since the simplex S^3 is invariant, we have $\mathscr{L}(S,E,I,R) \geq 0$.

Along a trajectory of system (1), $R_{n+1} = R_n(1+fI_n)$, and therefore

$$\begin{aligned}\Delta\mathscr{L} &= \mathscr{L}(x^{(n+1)}) - \mathscr{L}(x^{(n)}) \\ &= -(R_{n+1} - R_n) = -fR_nI_n \leq 0.\end{aligned}$$

Thus $\mathscr{L}$ is nonincreasing along every trajectory

in the simplex.

Moreover, $\Delta\mathscr{L} = 0$ whenever $R_n I_n = 0$.

For an interior trajectory, $R_n > 0$, and hence

$$\Delta\mathscr{L} = 0 \quad \Longrightarrow \quad I_n = 0.$$

Proposition 26. *The function $\mathscr{L}(S,E,I,R) = 1 - R$ is a Lyapunov-type function for the discrete SEIR Lotka–Volterra operator. In particular, it describes the irreversible transfer of mass toward the recovered component.*

Proof. The relation $\Delta\mathscr{L} = -fRI \le 0$ shows that $\mathscr{L}$ is nonincreasing along all trajectories. Hence the recovered component R_n is nondecreasing, while the total mass outside the recovered class, $S_n + E_n + I_n$, is nonincreasing. □

The Lyapunov-type dissipation alone does not determine the entire limiting point on the boundary. The global convergence theorem proved above provides the stronger conclusion that every interior trajectory satisfies

$$V^n(x^{(0)}) \longrightarrow (0, E_\infty, 0, 1 - E_\infty) \in Q,$$

where $0 \le E_\infty \le \frac{f}{d+f}$.

Thus the Lyapunov-type monotonicity is fully consistent with the global convergence toward the fixed segment Q. □

Proposition 27 (Local epidemic thresholds via the Jacobian)**.** *The local growth or decay of a small infectious perturbation can be characterized by the spectrum of the Jacobian matrix.*

For the operator (1), the Jacobian has the form

$$J(S,E,I,R) = \begin{pmatrix} 1 - aE - bI & -aS & -bS & 0 \\ aE & 1 + aS - dI & -dE & 0 \\ bI & dI & 1 + bS + dE - fR & -fI \\ 0 & 0 & fR & 1 + fI \end{pmatrix}.$$

First, consider a fixed point on the edge $[e_1, e_4]$,

$$x^* = (S^*, 0, 0, R^*), \qquad S^* + R^* = 1.$$

At this point,

$$J(x^*) = \begin{pmatrix} 1 & -aS^* & -bS^* & 0 \\ 0 & 1 + aS^* & 0 & 0 \\ 0 & 0 & 1 + bS^* - fR^* & 0 \\ 0 & 0 & fR^* & 1 \end{pmatrix}.$$

Hence the eigenvalue associated with the infectious direction is $\lambda_I = 1 + bS^* - fR^*$.

Therefore, a small infectious perturbation decreases locally when $\lambda_I < 1$, that is, $bS^* < fR^*$, whereas it may increase when $bS^* > fR^*$. The threshold condition $\lambda_I = 1$ is equivalent to $bS^* = fR^*$. Using $S^* + R^* = 1$, we obtain

$$S^* = \frac{f}{b+f}, \qquad R^* = \frac{b}{b+f}.$$

Thus the threshold point is $M = \left(\frac{f}{b+f}, 0, 0, \frac{b}{b+f}\right)$.

Similarly, consider a fixed point on the edge $[e_2, e_4]$,

$$x^* = (0, E^*, 0, R^*), \qquad E^* + R^* = 1.$$

The Jacobian becomes

$$J(x^*) = \begin{pmatrix} 1 - aE^* & 0 & 0 & 0 \\ aE^* & 1 & -dE^* & 0 \\ 0 & 0 & 1 + dE^* - fR^* & 0 \\ 0 & 0 & fR^* & 1 \end{pmatrix}.$$

The eigenvalue corresponding to the infectious direction is $\lambda_I = 1 + dE^* - fR^*$.

Hence a small infectious perturbation decreases locally if $dE^* < fR^*$, and may increase if $dE^* > fR^*$.

The threshold condition $\lambda_I = 1$ gives $dE^* = fR^*$.

Together with $E^* + R^* = 1$, this yields

$$E^* = \frac{f}{d+f}, \qquad R^* = \frac{d}{d+f}.$$

Therefore the corresponding threshold point is $N = \left(0, \frac{f}{d+f}, 0, \frac{d}{d+f}\right)$.

Thus the discrete SEIR Lotka-Volterra model does not require the introduction of the heuristic quantity $(a+b)/f$. Instead, the Jacobian spectrum yields two natural local threshold conditions, $bS^* = fR^*$ and $dE^* = fR^*$, corresponding precisely to the boundary points M and N. □

Numerical illustrations

To illustrate the analytical results, numerical iterations of the discrete SEIR Lotka–Volterra operator were performed for the representative parameter values

$$a = 0.8, \qquad b = 0.2, \qquad d = 0.4, \qquad f = 0.7.$$

These values satisfy the admissibility conditions $0 < a, b, d, f \leq 1$.

We considered the following three interior initial states:

$$x_1^{(0)} = (0.40, 0.20, 0.10, 0.30),$$

$$x_2^{(0)} = (0.25, 0.30, 0.20, 0.25),$$

and

$$x_3^{(0)} = (0.60, 0.10, 0.15, 0.15).$$

For each initial condition, all coordinates are positive and their sum is equal to one.

The numerical values obtained after 10, 50, and 100 iterations are presented in Table 3.

Table 3 – Numerical iterations for $a = 0.8$, $b = 0.2$, $d = 0.4$, and $f = 0.7$.

Init.	n	S_n	E_n	I_n	R_n
$x_1^{(0)}$	10	7.97×10^{-3}	0.458693	3.76×10^{-2}	0.495707
	50	2.81×10^{-10}	0.431014	2.02×10^{-6}	0.568984
	100	1.85×10^{-19}	0.431012	5.56×10^{-12}	0.568988
$x_2^{(0)}$	10	6.87×10^{-3}	0.320208	3.53×10^{-2}	0.637604
	50	6.35×10^{-8}	0.313491	1.00×10^{-9}	0.686509
	100	3.41×10^{-14}	0.313491	2.97×10^{-19}	0.686509
$x_3^{(0)}$	10	2.42×10^{-2}	0.382723	0.135110	0.457938
	50	1.03×10^{-7}	0.323409	1.71×10^{-8}	0.676590
	100	3.24×10^{-14}	0.323410	1.17×10^{-17}	0.676590

Numerical verification of signature transitions.

To verify the signature-transition structure, we additionally computed the separating functions along each numerical trajectory:

$$h_2(x^{(n)}) = aS_n - dI_n,$$

$$h_3(x^{(n)}) = bS_n + dE_n - fR_n.$$

The signature region at each iteration was identified from the simultaneous signs of these two functions.

The first trajectory starts in F_3 and enters F_4 at iteration $n = 8$.

The second trajectory follows the signature sequence

$$F_3 \longrightarrow F_4 \longrightarrow F_3,$$

with transitions occurring at $n = 3$ and $n = 18$, respectively.

The third trajectory follows

$$F_1 \longrightarrow F_3 \longrightarrow F_4 \longrightarrow F_3,$$

Table 4 – Numerically observed signature transitions for the three initial states.

Init.	n	$h_2(x^{(n)})$	$h_3(x^{(n)})$	Region
$x_1^{(0)}$	7	0.003534	-0.120608	F_3
	8	-0.003883	-0.135223	F_4
$x_2^{(0)}$	2	0.022278	-0.059345	F_3
	3	-0.005469	-0.094981	F_4
	17	-0.000073	-0.353233	F_4
	18	0.000024	-0.353932	F_3
$x_3^{(0)}$	5	0.090123	0.002115	F_1
	6	0.037682	-0.021069	F_3
	7	0.000897	-0.050726	F_3
	8	-0.021288	-0.085650	F_4
	29	-0.000004	-0.344126	F_4
	30	0.000001	-0.344170	F_3

with transitions occurring at $n = 6$, $n = 8$, and $n = 30$.

Numerical example of a direct $F_1 \to F_4$ transition. To illustrate Proposition 22, consider the same parameter values

$$(a, b, d, f) = (0.8, 0.2, 0.4, 0.7)$$

and the interior initial point

$$x^{(0)} = (0.31125, 0.00025, 0.60225, 0.08625).$$

The separating functions at this point satisfy

$$h_2(x^{(0)}) = 0.008100 > 0, h_3(x^{(0)}) = 0.001975 > 0.$$

Hence $x^{(0)}$ belongs to the strict region F_1.

After one iteration, we obtain

$$x^{(1)} = \big(0.2736976875,\ 0.000252025,\ 0.60343944375,\ 0.12261084375\big).$$

Direct calculation gives

$$h_2(x^{(1)}) = -0.0224176275 < 0,$$

$$h_3(x^{(1)}) = -0.030987243125 < 0.$$

Consequently, $x^{(1)}$ belongs to the strict region F_4. Therefore,

$$F_1 \longrightarrow F_4$$

is a realizable one-step transition, despite the absence of a common facet between these two regions. This numerical example confirms the analytical result of Proposition 22.

Additional numerical examples of one-step transitions.

We now illustrate two further transitions using the same parameter values $(a,b,d,f) = (0.8,0.2,0.4,0.7)$.

First, consider $x^{(0)} = (0.28,0.15,0.536,0.034)$. The separating functions are

$$h_2(x^{(0)}) = 0.009600 > 0,$$

$$h_3(x^{(0)}) = 0.092200 > 0.$$

Thus, $x^{(0)}$ belongs to the strict signature region F_1.

After one iteration,

$$V(x^{(0)}) = \big(0.216384,\ 0.151440,\ 0.5854192,\ 0.0467568\big).$$

Consequently,

$$h_2(V(x^{(0)})) = -0.06106048 < 0,$$

$$h_3(V(x^{(0)})) = 0.07112304 > 0.$$

Therefore, the one-step transition $F_1 \longrightarrow F_2$ is realized.

Next, consider

$$x^{(0)} = (0.0004,0.4381,0.3237,0.2378).$$

For this point,

$$h_2(x^{(0)}) = -0.129160 < 0,$$

$$h_3(x^{(0)}) = 0.008860 > 0.$$

Hence $x^{(0)}$ belongs to the strict signature region F_2.

After one iteration, we obtain

$$h_2(V(x^{(0)})) < 0, \qquad h_3(V(x^{(0)})) < 0.$$

Thus, the image belongs to the strict region F_4, giving $F_2 \longrightarrow F_4$.

These examples demonstrate the realizability of the transitions $F_1 \to F_2$ and $F_2 \to F_4$ for interior initial states.

Numerical example of an $F_3 \to F_1$ transition.

Consider the parameter values

$$(a,b,d,f) = (0.8,0.2,0.4,0.7)$$

and the interior initial state

$$x^{(0)} = \big(0.0327042864,\ 0.6094817850,\ 0.0000264597,\ 0.3577874689\big).$$

The separating functions satisfy

$$h_2(x^{(0)}) > 0, \qquad h_3(x^{(0)}) < 0.$$

Thus $x^{(0)}$ belongs to F_3.

After one iteration,

$$h_2(V(x^{(0)})) > 0, \qquad h_3(V(x^{(0)})) > 0.$$

Hence the image belongs to F_1, which verifies the transition

$$F_3 \longrightarrow F_1.$$

These numerical results demonstrate that the signature regions are not necessarily visited in a single fixed order. In particular, the observed transition $F_4 \to F_3$ confirms that no universal one-way direction can be imposed between these two regions under the general parameter assumptions.

The numerical transitions are consistent with the analytical one-step sign conditions derived in the preceding section. They also illustrate that the signature-transition analysis provides information about the intermediate trajectory geometry that is not captured by the global convergence theorem alone.

Table 3 shows that the susceptible component S_n decreases toward zero, whereas the recovered component R_n increases along each of the three trajectories. The infectious component I_n also tends to zero. At the same time, the exposed component E_n approaches a nonzero limiting value depending on the initial condition.

For the chosen parameter values,

$$\frac{f}{d+f} = \frac{0.7}{0.4+0.7} \approx 0.636364.$$

The limiting exposed components obtained numerically are approximately $E_\infty^{(1)} = 0.431012$, $E_\infty^{(2)} = 0.313491$, $E_\infty^{(3)} = 0.323410$.

Thus, in all three cases,

$$0 \le E_\infty^{(j)} \le \frac{f}{d+f}, \qquad j = 1,2,3.$$

Consequently, the corresponding limiting states are approximately

$$x_\infty^{(1)} = (0, 0.431012, 0, 0.568988),$$

$$x_\infty^{(2)} = (0, 0.313491, 0, 0.686509),$$

and

$$x_\infty^{(3)} = (0, 0.323410, 0, 0.676590).$$

Each of these points belongs to the fixed segment

$$Q = \left\{ (0, E, 0, 1-E) : 0 \le E \le \frac{f}{d+f} \right\}.$$

Hence the numerical experiments are consistent with the global convergence theorem. They also illustrate an important feature of the model: different interior initial conditions may converge to different points of the same fixed segment Q, rather than to a single equilibrium common to all trajectories.

Parameter sensitivity analysis. To complement the numerical experiments above, a simple one-at-a-time parameter sensitivity analysis was performed. The initial state was fixed at

$$x^{(0)} = (0.40, 0.20, 0.10, 0.30),$$

and the baseline parameter set was chosen as

$$(a, b, d, f) = (0.8, 0.2, 0.4, 0.7).$$

Each parameter was then increased separately while the remaining three parameters were kept at their baseline values. The corresponding limiting values of the exposed component are reported in Table 5.

The results show that the limiting point on the fixed boundary segment depends not only on the initial condition but also on the interaction parameters. For the selected perturbations, increasing a, b, or d decreases the limiting exposed fraction E_∞, whereas increasing f increases it. Among the considered one-at-a-time changes, the variation in d produces the largest decrease in E_∞. These numerical observations are specific to the chosen baseline state and parameter perturbations and should not be interpreted as global monotonicity properties with respect to the parameters.

Table 5 – One-at-a-time parameter sensitivity analysis for the limiting exposed component E_∞, with all non-varied parameters fixed at their baseline values.

Case	a	b	d	f	E_∞
Baseline	0.8	0.2	0.4	0.7	0.431012
a increased	0.9	0.2	0.4	0.7	0.427759
b increased	0.8	0.3	0.4	0.7	0.412999
d increased	0.8	0.2	0.5	0.7	0.376360
f increased	0.8	0.2	0.4	0.8	0.464525

In all considered cases, the numerical trajectory still converges to a point of the corresponding fixed boundary segment Q, with the endpoint of Q determined by the respective values of d and f. This is consistent with the analytical global convergence result.

CONCLUSION

In the present study, a discrete SEIR-type model formulated within the framework of Lotka-Volterra operators was investigated on the three-dimensional simplex. The model describes nonlinear interactions among susceptible, exposed, infectious, and recovered population fractions while preserving the simplex structure.

The simplex was decomposed into four convex polyhedral signature regions. Their geometric facet-adjacency structure was determined, and one-step sign conditions were derived to distinguish geometric adjacency from actual dynamical transitions. The analysis also demonstrated that direct transitions between non-facet-adjacent regions must be examined separately.

The main global result establishes that every trajectory starting from an interior point of the simplex converges to a single point of the fixed

segment

$$Q = \left\{ (0, E, 0, 1-E) : 0 \le E \le \frac{f}{d+f} \right\}.$$

More precisely,

$$V^n(x^{(0)}) \longrightarrow (0, E_\infty, 0, 1-E_\infty), \quad 0 \le E_\infty \le \frac{f}{d+f}.$$

Thus, the limiting equilibrium generally depends on the initial condition, and interior trajectories need not converge to a common boundary equilibrium.

The spectral analysis identified local infectious threshold conditions through the Jacobian multipliers along the fixed boundary sets. The numerical experiments illustrated convergence to different points of Q and verified selected transitions between signature regions through the signs of the separating functions. The one-at-a-time sensitivity analysis also showed that, for the considered parameter perturbations, the limiting equilibrium depends on the interaction coefficients.

These results demonstrate that the discrete Lotka-Volterra framework, combined with signature-based geometric analysis, provides a systematic approach to distinguishing polyhedral adjacency, local one-step transitions, and global asymptotic behavior in SEIR-type dynamical systems.

Future research may address calibration using epidemiological observations, the incorporation of demographic and spatial effects, and extensions to more detailed compartmental models.

Acknowledgment

The authors thank the reviewers for their valuable comments and suggestions.

Author Contributions: Conceptualization, D. E and D. X; methodology, D. E and D. X; formal analysis, D. E and D. X; investigation, D. E and D. X; writing-original draft, D. X; writing-review and editing, D. E and D. X; supervision, D. E.

References

[1] Anderson, R. M. and R. M. May. *Infectious Diseases of Humans: Dynamics and Control*. Oxford University Press, 1991.

[2] Hethcote, H. W. "The mathematics of infectious diseases." *SIAM Review* 42, no. 4 (2000): 599–653. https://doi.org/10.1137/S0036144500371907

[3] Liu, Q., D. Jiang, N. Shi, T. Hayat, and A. Alsaedi. "Asymptotic behavior of a stochastic delayed seir epidemic model with nonlinear incidence." *Physica A: Statistical Mechanics and its Applications* 462 (2016): 870–882. https://doi.org/10.1016/j.physa.2016.06.095

[4] Shao, P. and S. Shateyi. "Stability analysis of seirs epidemic model with nonlinear incidence rate function." *Mathematics* 9, no. 21 (2021): 2644. https://doi.org/10.3390/math9212644

[5] Eshmamatova, D. B. and M. A. Tadzhieva. "Analysis and classification of fixed points of operators on a simplex." *Bulletin of the Karaganda University. Mathematics Series* 120, no. 4 (2025): 107–124. https://doi.org/10.31489/2025M4/107-124

[6] Eshmamatova, D. B. "Dynamics of a discrete sird model based on lotka-volterra mappings." *AIP Conference Proceedings* 3045 (2024): 020005. https://doi.org/10.1063/5.0199863

[7] Ganikhodzhaev, R., D. Eshmamatova, M. Tadzhieva, and B. Zakirov. "Some degenerate cases of discrete lotka-volterra dynamical systems and their applications in epidemiology." *Journal of Mathematical Sciences* 289, no. 5 (2025): 755–769. https://doi.org/10.1007/s10958-024-07404-6

[8] Ghosh, D., P. K. Santra, G. S. Mahapatra, A. Elsonbaty, and A. A. Elsadany. "A discrete-time epidemic model for the analysis of transmission of covid19 based upon data of epidemiological parameters." *The European Physical Journal Special Topics* 231, no. 18–20 (2022): 3461–3470. https://doi.org/10.1140/epjs/s11734-022-00537-2

[9] Grant, A. "Dynamics of COVID-19 epidemics: SEIR models underestimate peak infection rates and overestimate epidemic duration." *medRxiv* (2020): 1–16. https://doi.org/10.1101/2020.04.02.20050674

[10] Ak Gümüş, Ö., Q. Cui, G. M. Selvam, and A. Vianny. "Global stability and bifurcation analysis of a discrete time sir epidemic model." *Miskolc Mathematical Notes* 23, no. 1 (2022): 193–210. https://doi.org/10.18514/MMN.2022.3417

[11] Shoyimardonov, S. K. and U. A. Rozikov. "Discrete-time dynamical systems generated by a quadratic operator." *Russian Journal of Nonlinear Dynamics* 21, no. 3 (2025): 399–418. https://doi.org/10.20537/nd250803

[12] Saburov, M. "On the surjectivity of quadratic stochastic operators acting on the simplex." *Mathematical Notes* 99, no. 3–4 (2016): 623–627. https://doi.org/10.1134/S0001434616030391

[13] Zeeman, E. C. and M. L. Zeeman. "From local to global behavior in competitive lotka-volterra systems." *Transactions of the American Mathematical Society* 355, no. 2 (2003): 713–734. https://doi.org/10.1090/S0002-9947-02-03103-3

[14] Martcheva, M. *An Introduction to Mathematical Epidemiology*. ser. Texts in Applied Mathematics, Vol. 61. Springer, 2015. https://doi.org/10.1007/978-1-4899-7612-3

[15] Galor, O. *Discrete Dynamical Systems*. Berlin, Heidelberg: Springer, 2007. https://doi.org/10.1007/3-540-36776-4

[16] Barnsley, M. F. and A. Vince. "The conley attractors of an iterated function system." *Bulletin of the Australian Mathematical Society* 88, no. 2 (2013): 267–279. https://doi.org/10.1017/S0004972713000348

[17] Sánchez-Gabites, J. J. "Unstable attractors in manifolds." *Transactions of the American Mathematical Society* 362, no. 7 (2010): 3563–3589. https://doi.org/10.1090/S0002-9947-10-05061-0

[18] Sangotola, A. O., O. A. Akinwumi, O. A. Nuga, E. A. Adebayo, A. E. Adeniji, and A. J. Adigun. "An seir epidemic model with two infectious pathways." *Communications in Mathematical Biology and Neuroscience* 2023 (2023): 133. https://doi.org/10.28919/cmbn/8089

Information about authors

Dilfuza Eshmamatova *– DSc, Professor, Tashkent State Transport University and Romanovsky Institute of Mathematics, Tashkent, Uzbekistan, e-mail: 24dil@mail.ru*
Dildora Xakimova *– PhD student, Tashkent State Transport University, Tashkent, Uzbekistan, e-mail: xakimovadildora47@gmail.com*